 CMES, vol.80, no.3, pp.219-232, 2011

A Spectrally Accurate Quadrature for 3-D Boundary Integrals

Gregory Baker[1] **and Huaijian Zhang**[1]

Abstract: Boundary integral methods have proved very useful in the simulation of free surface motion, in part, because only information at the surface is necessary to track its motion. However, the velocity of the surface must be calculated quite accurately, and the error must be reasonably smooth, otherwise the surface buckles as numerical inaccuracies grow, leading to a failure in the simulation. For two-dimensional motion, the surface is just a curve and the boundary integrals are simple poles that may be removed, allowing spectrally accurate numerical integration. For three-dimensional motion, the singularity in the integrand, although weak, presents a greater challenge to the design of spectrally accurate quadrature. One way forward is to take advantage of a polar coordinate representation around the singularity point. Of course the typical grids used in boundary integral methods don't lend themselves to transformation to local polar coordinates, but the range of integration can be split into two regions, one near the singularity where polar coordinates can be used with suitable interpolation and an outer region where standard methods apply. We provide details and results of some tests that confirm spectral accuracy in the method.

Keywords: Free Surface Flows, Singular Integrals, Vortex Methods, Spectral Accuracy.

1 Introduction

The use of boundary integrals for tracking free surface flows in incompressible, inviscid fluids is now well established. The simplest case, that of a fluid adjacent to a vacuum, can be treated simply as the formulation of a boundary integral to solve Laplace's equation, see for example Beale (2001). More generally, the boundary integrals arise as dipole sheets or vortex sheets from the transport of vorticity, see for example Baker (2010).

[1] Department of Mathematics, The Ohio State University, 231 W. 18th Ave, Columbus, OH43210, baker@math.ohio-state.edu

The Euler equations of motion in vorticity form are:

$$\frac{\partial \omega}{\partial t} + \mathbf{u} \cdot \nabla \omega = \omega \cdot \nabla \mathbf{u}, \tag{1}$$

$$\nabla \cdot \mathbf{u} = 0, \tag{2}$$

where the velocity is $\mathbf{u}$ and the vorticity $\omega = \nabla \times \mathbf{u}$.

The velocity may be determined from the vorticity by the Biot-Savart integral Saffman (1992),

$$\mathbf{u}(\mathbf{x},t) = -\int \omega(\mathbf{x}',t) \times \nabla G(\mathbf{x}-\mathbf{x}')\, \mathrm{d}\mathbf{x}', \tag{3}$$

where G is the free-space Green's function for Laplace's equation. The result is valid in the absence of solid boundaries, but additional contribution to the velocity can be added to account for them. If ω is known at some time t, then (3) can be integrated to determine $\mathbf{u}$ and then (1) can be advanced in time to update ω. Clearly, the method is well-suited for representing the vorticity at a collection of Lagrangian markers that then track with the fluid velocity. Only points where the vorticity is non-zero need be tracked.

An important special case is when the vorticity is distributed as a delta function along a surface

$$\omega = \gamma \delta(n), \quad \text{subject to } \mathbf{n} \cdot \gamma = 0, \tag{4}$$

where n is the distance along the normal $\mathbf{n}$ to the surface and γ is called the vortex sheet strength. Since the vorticity must point along a tangent to the surface, we may write

$$\gamma = \gamma \mathbf{t}, \tag{5}$$

where $\mathbf{t}$ is a unit tangent vector. As a consequence, the fluid velocity can be expressed as

$$\mathbf{u}(\mathbf{x},t) = \int \gamma(p,q) \nabla G\big(\mathbf{x}-\mathbf{x}(p,q)\big) \times \mathbf{t}(p,q)\, \mathrm{d}S(p,q), \tag{6}$$

where the surface location is written in parametric form $\mathbf{x}(p,q)$.

There are several important properties of vortex sheets that are obtained by taking the limit as $\mathbf{x} \to \mathbf{x}(\eta,\zeta)$, a point on the surface, along the normal there. The result is

$$\mathbf{u}_{\pm}(\eta,\zeta) = \mathbf{u}_P(\eta,\zeta) \pm \frac{\gamma(\eta,\zeta)}{2}\, \mathbf{n}(\eta,\zeta) \times \mathbf{t}(\eta,\zeta), \tag{7}$$

where the negative subscript is from the side into which the normal points and

$$\mathbf{u}_P(\eta,\zeta) = \int \gamma(p,q)\,\nabla G\big(\mathbf{x}(\eta,\zeta)-\mathbf{x}(p,q)\big)\times\mathbf{t}(p,q)\,\mathrm{d}S(p,q) \tag{8}$$

is a principal-valued integral. Thus the vortex sheet strength measures the jump in tangential components of the velocity across the surface,

$$\gamma(p,q)\,\mathbf{n}(p,q)\times\mathbf{t}(p,q) = \mathbf{u}_+(p,q)-\mathbf{u}_-(p,q)\,, \tag{9}$$

while the normal components are continuous,

$$\mathbf{n}(p,q)\cdot\mathbf{u}_+ = \mathbf{n}(p,q)\cdot\mathbf{u}_- = \mathbf{n}(p,q)\cdot\mathbf{u}_P\,. \tag{10}$$

The nature of vortex sheets lends itself to a representation for free surfaces between immiscible fluids because the normal component of the fluid velocity is automatically continuous and the jump in tangential component captures the generation of vorticity in the presence of a jump in densities. Indeed, a vortex sheet can be viewed as a free surface between two immiscible fluids of equal densities where there is no generation of vorticity and the vortex sheet merely advects with the average fluid velocity at the surface. The extension to fluids with different densities on either side of the surface has been derived in two-dimensional motion Baker (1982) and in three-dimensional motion Baker et al (1984); a comprehensive treatment is also available Baker (2010). What these studies also show is that spectrally accurate methods are easily obtainable in two-dimensional motion because the pole singularity in (12) can be removed leaving the integrand analytic. The 3/2-power singularity in (8) cannot be removed completely by analytic techniques, although it can be weakened further Baker et al (1984). The challenge is to find accurate numerical methods for the integration (8) that give errors that are smooth, avoiding artificial buckling of the surface as it moves with the calculated velocity.

One way forward has been suggested by an appropriate regularization of the Green's function and tested thoroughly for two-dimensional motion with good success Baker and Beale (2004). A version has been proposed for three-dimensional motion Beale (2001) with a specific application to deep water waves. Results were reported last year Baker and Zhang (2010) that confirm the expected third-order convergence in the grid spacing, but in applications to deep water waves, this accuracy is not enough. Instead, a spectral accurate method has been designed based on an approach used in electromagnetic scattering from surfaces Bruno and Kunyansky (2001). The method is described here specifically for vortex sheets and results from tests confirm spectral accuracy.

2 Polar coordinate transformation

The singularity in the integrand of (8) can be weakened from $1/r^2$ to $1/r$ where $r = |\mathbf{x}(\eta,\zeta) - \mathbf{x}(p,q)|$ by exploiting the vector identity

$$\mathbf{a} \times (\mathbf{b} \times \mathbf{c}) = \mathbf{b}\,(\mathbf{a}\cdot\mathbf{c}) - (c)\,(\mathbf{a}\cdot\mathbf{b}) \tag{11}$$

and the surface integrals

$$\int \nabla G(\mathbf{x}(\eta,\zeta) - \mathbf{x}(p,q)) \cdot \mathbf{n}(p,q)\,\mathrm{d}S(p,q) = -\frac{1}{2}, \tag{12}$$

$$\int \nabla G(\mathbf{x}(\eta,\zeta) - \mathbf{x}(p,q)) \times \mathbf{n}(p,q)\,\mathrm{d}S(p,q) = 0\,. \tag{13}$$

The result in (12) depends on the geometry. The integral is zero when the surface is topologically flat, and takes the value shown when it is closed or topologically cylindrical.

The first step is to use (11) to write

$$\begin{aligned}\nabla G(\mathbf{x}(\eta,\zeta) - \mathbf{x}(p,q)) \times \mathbf{t}(p,q) = {} & \big[\nabla G(\mathbf{x}(\eta,\zeta) - \mathbf{x}(p,q)) \cdot \mathbf{n}(p,q)\big]\,\mathbf{s}(p,q) \\ & - \big[\nabla G(\mathbf{x}(\eta,\zeta) - \mathbf{x}(p,q)) \times \mathbf{n}(p,q)\big] \times \mathbf{s}(p,q)\end{aligned}$$

where $\mathbf{s} = \mathbf{n} \times \mathbf{t}$. Then the integral in (8) can be replaced by the two integrals,

$$\begin{aligned}\mathbf{u}_P = {} & \int \big[\gamma(p,q)\,\mathbf{s}(p,q) - \gamma(\eta,\zeta)\,\mathbf{s}(\eta,\zeta)\big]\,\big[\nabla G\big(\mathbf{x}(\eta,\zeta) \\ & - \mathbf{x}(p,q)\big) \cdot \mathbf{n}(p,q)\big]\,\mathrm{d}S(p,q) - \frac{\gamma(\eta,\zeta)\,\mathbf{s}(\eta,\zeta)}{2} \\ & + \int \big[\gamma(p,q)\,\mathbf{s}(p,q) - \gamma(\eta,\zeta)\,\mathbf{s}(\eta,\zeta)\big] \times \big[\nabla G\big(\mathbf{x}(\eta,\zeta) - \mathbf{x}(p,q)\big) \times \mathbf{n}(p,q)\big]\,\mathrm{d}S(p,q)\end{aligned} \tag{14}$$

and there is an additional zero in the numerator of each integrand that weakens the singularity at $\mathbf{x}(\eta,\zeta)$.

The value in weakening the singularity becomes transparent when polar coordinates are introduced;

$$p = \eta + \rho\,\cos(\theta)\,, \quad q = \zeta + \rho\,\sin(\theta)\,. \tag{15}$$

Note in particular that

$$\begin{aligned}\mathbf{x}(p,q) - \mathbf{x}(\eta,\zeta) &\approx \rho\left(\frac{\partial \mathbf{x}}{\partial p}(\eta,\zeta)\,\cos(\theta) + \frac{\partial \mathbf{x}}{\partial q}(\eta,\zeta)\,\sin(\theta)\right) + \mathrm{O}\big(\rho^2\big) \\ &\approx \rho\,\mathbf{D}(\eta,\zeta,\theta) + \mathrm{O}\big(\rho^2\big)\,.\end{aligned} \tag{16}$$

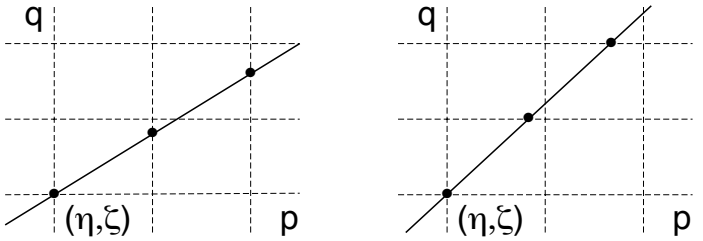

Figure 1: A diagram illustrating two cases where a constant θ line intersects the grid

Similarly,

$$\gamma(p,q)\,\mathbf{s}(p,q) - \gamma(\eta,\zeta)\,\mathbf{s}(\eta,\zeta) \approx \rho\,\mathbf{N}(\eta,\zeta,\theta) + \mathrm{O}\left(\rho^2\right), \tag{17}$$

As a result, for small ρ, the integrands in (16) become

$$(\rho\,\mathbf{N})\,\frac{(\rho\,\mathbf{D}\cdot\mathbf{n})}{\left(\rho^3\,|\mathbf{D}|^3\right)} \quad \text{and} \quad (\rho\,\mathbf{N})\,\frac{(\rho\,\mathbf{D}\times\mathbf{n})}{\left(\rho^3\,|\mathbf{D}|^3\right)}$$

and since $\mathrm{d}S(p,q) = \rho\,\mathrm{d}\rho\,\mathrm{d}\theta$, the singularities have been removed and the integrands are smooth function of ρ and θ.

However, the surface is typically represented as a rectangular grid in the surface parameters (p,q) and not in (ρ,θ). To apply the trapezoidal integration, equally spaced points are needed in ρ and θ and numerical interpolation will be needed to obtain theses values, a potentially costly process. Fortunately, there is a way to proceed that keeps the costs to reasonable levels and with spectral accuracy.

Consider how a constant θ line intersects the rectangular grid in (p,q). Fig. 1 illustrates two possible cases. Let h_1, h_2 be the uniform grid spacing in p,q respectively. On the left, the constant θ line crosses the constant p lines with a uniform spacing $h_\rho = h_1/\cos(\theta)$ in ρ. Interpolated values for $\mathbf{x}$, γ, $\mathbf{s}$, $\mathbf{t}$, $\mathbf{n}$ can now be obtained using information only along the constant p line. In contrast, the case on the right in Fig. 1 shows equally spacing $h_\rho = h_2/\sin(\theta)$ in ρ as the constant θ lines cross the constant q lines. Interpolation now is needed only along lines of constant q.

The procedure to integrate the integrals in (14) numerically in polar coordinates can now be stated. For convenience the procedure will be described for the first integral in (14); the other integral is treated in similar fashion. The integration in ρ

is performed first with θ fixed. In other words, the trapezoidal rule is applied to

$$I(\theta) = \int_{-\infty}^{\infty} \left[\gamma(p,q)\,\mathbf{s}(p,q) - \gamma(\eta,\zeta)\,\mathbf{s}(\eta,\zeta)\right] \left[\nabla G\big(\mathbf{x}(\eta,\zeta) - \mathbf{x}(p,q)\big)\cdot \mathbf{n}(p,q)\right] \rho \,\mathrm{d}\rho \tag{18}$$

If $-\theta_s < \theta < \theta_s$ or $\pi - \theta_s < \theta < \pi + \theta_s$ where $\tan(\theta_s) = h_2/h_1$, then the choice $h_\rho = h_1/\cos(\theta)$ is made and the trapezoidal rule is applied at $\rho_k = kh_\rho$. As illustrated in the diagram on the left in Fig. 1, the quadrature points will occur at $(kh_1, kh_\rho \sin(\theta))$ and the quantities needed to evaluate the integrand must be interpolated at the points along the constant $p = kh_1$ lines. Let the subscript k refer to these interpolated values. Alternately, if $\theta_s < \theta < \pi - \theta_s$ or $-\pi + \theta_s < \theta < -\theta_s$, then the choice $h_\rho = h_2/\sin(\theta)$ leads to quadrature points at $(kh_\rho \cos(\theta), kh_2)$. Interpolated values must now be obtained along $q = kh_2$ lines. In either case, the approximation to (18) becomes

$$I(\theta) = h_\rho \sum_{k=-\infty}^{\infty} \rho_k \left[\gamma_k \mathbf{s}_k - \gamma(\eta,\zeta)\,\mathbf{s}(\eta,\zeta)\right] \left[\nabla G\big(\mathbf{x}(\eta,\zeta) - \mathbf{x}_k\big)\cdot \mathbf{n}_k\right] \tag{19}$$

Note that the value of the integrand at $\rho = 0$ must be determined as the limit of an indeterminate form.

The final step is the integration in θ. Set $\theta = \theta_j = jh_\theta$ where $h_\theta = 2\pi/K$ and apply the trapezoidal rule.

$$\begin{aligned} &\int \left[\gamma(p,q)\,\mathbf{s}(p,q) - \gamma(\eta,\zeta)\,\mathbf{s}(\eta,\zeta)\right] \left[\nabla G\big(\mathbf{x}(\eta,\zeta) - \mathbf{x}(p,q)\big)\cdot \mathbf{n}(p,q)\right] \mathrm{d}S(p,q) \\ &= \int_0^{\pi} I(\theta)\,\mathrm{d}\theta \\ &\approx h_\theta \sum_{j=0}^{K/2-1} I(\theta_j) \end{aligned} \tag{20}$$

Note that the range in θ is only $(0,\pi)$ because the range in ρ already covers the rest of the range in θ. Since $I(\theta+\pi) = I(\theta)$, the integrand is periodic and the trapezoidal rule is spectrally accurate.

An important refinement to the algorithm that reduces the costs of interpolation is to split the range of integration into two parts. Let $K(p,q)$ represent either of the integrands in (14) and write the integral with the following decomposition,

$$\int K(p,q)\,\mathrm{d}S(p,q) = \int K(p,q)\,T(\rho)\,\mathrm{d}S(p,q) + \int K(p,q)\left(1 - T(\rho)\right)\mathrm{d}S(p,q) \tag{21}$$

where $T(\rho)$ is a reasonably smooth transition from a disk surrounding the singularity in the integration to regions well away from the singularity. The choice made before Bruno and Kunyansky (2001) and used here as well is

$$T(\rho) = \begin{cases} 1\,, & \text{for } \rho \le r_1\,, \\ \exp\bigl(2\mathrm{e}^{-1/x}/(x-1)\bigr)\,, & \text{for } r_1 < \rho < r_2, \text{ where } x = (\rho - r_1)/(r_2 - r_1)\,, \\ 0\,, & \text{for } \rho \ge r_2\,. \end{cases} \tag{22}$$

The consequence is that the sum in (19) requires only the range $|\rho_k| < r_2$. The second integral in (21) can be evaluated at the regular grid points that lie outside $\rho = r_1$.

Provided the interpolation is performed with high accuracy, either spectrally or with high-order Hermite interpolation, the expectation is that the numerical integration will be spectrally accurate. We test this expectation by considering a simple test, used before to test the accuracy of blob methods Baker and Zhang (2010).

3 Test Case: A Cylindrical Vortex Sheet

The surface is given by

$$x(p,q) = R\cos(p)\,, \quad y(p,q) = R\sin(p)\,, \quad z(p,q) = q\,, \tag{23}$$

with corresponding surface vectors,

$$\mathbf{t}_1 = (0,0,1)\,, \quad \mathbf{t}_2 = (-\cos(p), \sin(p), 0)\,, \quad \mathbf{n} = (\cos(p), \sin(p), 0)\,. \tag{24}$$

The easiest way to construct velocity components (u_P, v_P, w_P) that correspond to a vortex sheet,

$$\gamma = \gamma_1(p,q)\,\mathbf{t}_1 + \gamma_2(p,q)\,\mathbf{t}_2\,, \tag{25}$$

is to introduce the velocity potential,

$$\mathbf{u} = \nabla\phi\,, \tag{26}$$

since $\nabla \times \mathbf{u} = 0$ away from the surface. By invoking (2), ϕ must satisfy Laplace's equation inside and outside the vortex sheet. Now simply make a choice, for example,

$$\phi = f(r)\cos(n\theta)\cos(\alpha z)\,, \tag{27}$$

where $f(r)$ must satisfy

$$r\frac{\mathrm{d}}{\mathrm{d}r}\left(r\frac{\mathrm{d}f}{\mathrm{d}r}\right)-(n^2+\alpha^2r^2)\,f=0\,, \tag{28}$$

the modified Bessel equation of integer order n. The appropriate choice of solutions, suitably normalized, are

$$f(r)=A\,\frac{I_n(\alpha r)}{\alpha I_n'(\alpha R)}\,, \qquad r<R\,, \tag{29}$$

$$f(r)=B\,\frac{K_n(\alpha r)}{\alpha K_n'(\alpha R)}\,, \qquad r>R\,. \tag{30}$$

The requirement that the normal component of the velocity is continuous on the surface (10) makes $A=B$. The jump in velocity across the surface is

$$\mathbf{u}_+-\mathbf{u}_-=\frac{A\Gamma_n}{\alpha R}\times \\ \big(-n\sin(p)\sin(np)\cos(\alpha q),n\cos(p)\sin(np)\cos(\alpha q),\alpha^2R\cos(np)\sin(\alpha q)\big)\,, \tag{31}$$

which must match vortex sheet strength through (9). Here,

$$\Gamma_n=\frac{I_n(\alpha R)}{I_n'(\alpha R}-\frac{K_n(\alpha R)}{K_n'(\alpha R)}\,. \tag{32}$$

Finally,

$$\gamma_1=-\frac{nA\Gamma_n}{\alpha R}\sin(np)\cos(\alpha q)\,, \tag{33}$$

$$\gamma_2=\alpha A\Gamma_n\cos(np)\sin(\alpha q)\,. \tag{34}$$

The vortex sheet distribution generates the surface velocity $\mathbf{u}_p$ by the regularized surface integral (14). In this specific example, the integral

$$\mathbf{I}=\int\big[\gamma(p,q)\,\mathbf{s}(p,q)-\gamma(\eta,\zeta)\,\mathbf{s}(\eta,\zeta)\big]\,\big[\nabla G\big(\mathbf{x}(\eta,\zeta)-\mathbf{x}(p,q)\big)\cdot\mathbf{n}(p,q)\big]\,\mathrm{d}S(p,q) \tag{35}$$

has components,

$$I_1 = \frac{R^2}{4\pi}\int_{-\infty}^{\infty}\int_0^{2\pi} \frac{\big(\gamma_1(\eta,\zeta)\,\sin(\eta) - \gamma_1(p,q)\,\sin(p)\big)\,\big(1-\cos(p-\eta)\big)}{D^3}\,\mathrm{d}p\,\mathrm{d}q\,, \tag{36}$$

$$I_2 = \frac{R^2}{4\pi}\int_{-\infty}^{\infty}\int_0^{2\pi} \frac{\big(\gamma_1(p,q)\,\cos(p) - \gamma_1(\eta,\zeta)\,\cos(\eta)\big)\,\big(1-\cos(p-\eta)\big)}{D^3}\,\mathrm{d}p\,\mathrm{d}q\,, \tag{37}$$

$$I_3 = \frac{R^2}{4\pi}\int_{-\infty}^{\infty}\int_0^{2\pi} \frac{\big(\gamma_2(\eta,\zeta) - \gamma_2(p,q)\big)\,\big(1-\cos(p-\eta)\big)}{D^3}\,\mathrm{d}p\,\mathrm{d}q\,, \tag{38}$$

where

$$D^2 = 2R^2\,\big(1-\cos(p-\eta)\big) + (q-\zeta)^2\,. \tag{39}$$

The other integral,

$$\mathbf{J} = \int \big[\gamma(p,q)\mathbf{s}(p,q) - \gamma(\eta,\zeta)\mathbf{s}(\eta,\zeta)\big] \times \big[\nabla G\big(\mathbf{x}(\eta,\zeta) - \mathbf{x}(p,q)\big) \times \mathbf{n}(p,q)\big]\,\mathrm{d}S(p,q)\,, \tag{40}$$

has components,

$$J_1 = \frac{R}{4\pi}\int_{-\infty}^{\infty}\int_0^{2\pi} \frac{-R\sin(p-\eta)\,\big(\gamma_1(p,q)\,\cos(p) - \gamma_1(\eta,\zeta)\,\cos(\eta)\big) + \cos(p)N}{D^3}\,\mathrm{d}p\,\mathrm{d}q\,, \tag{41}$$

$$J_2 = \frac{R}{4\pi}\int_{-\infty}^{\infty}\int_0^{2\pi} \frac{-R\sin(p-\eta)\,\big(\gamma_1(p,q)\,\sin(p) - \gamma_1(\eta,\zeta)\,\sin(\eta)\big) + \sin(p)N}{D^3}\,\mathrm{d}p\,\mathrm{d}q\,, \tag{42}$$

$$J_3 = -\frac{R}{4\pi}\int_{-\infty}^{\infty}\int_0^{2\pi} \frac{\gamma_1(\eta,\zeta)\,(q-\zeta)\,\sin(p-\eta)}{D^3}\,\mathrm{d}p\,\mathrm{d}q\,, \tag{43}$$

where

$$N = (q-\zeta)\,\big(\gamma_2(p,q) - \gamma(\eta,\zeta)\big)\,.$$

On the other hand, (7) means that $2\mathbf{u}_p = \mathbf{u}_+ + \mathbf{u}_-$, or $\mathbf{u}_p = (u_P, v_P, w_P)$ where

$$2u_P(\eta,\zeta) = 2A\cos(\eta)\cos(n\eta)\cos(\alpha\zeta) + \frac{nAV_n}{\alpha R}\sin(\eta)\sin(n\eta)\cos(\alpha\zeta), \quad (44)$$

$$2v_P(\eta,\zeta) = 2A\sin(\eta)\cos(n\eta)\cos(\alpha\zeta) - \frac{nAV_n}{\alpha R}\cos(\eta)\sin(n\eta)\cos(\alpha\zeta), \quad (45)$$

$$2w_p(\eta,\zeta) = -AV_n\cos(n\eta)\sin(\alpha\zeta), \quad (46)$$

where

$$V_n = \frac{I_n(\alpha R)}{I_n'(\alpha R} + \frac{K_n(\alpha R)}{K_n'(\alpha R)} \quad (47)$$

The choice for γ_1 (33) and γ_2 (34) will produce the velocity components given above. This, then, provides a test case for the numerical integration of the boundary integrals (14).

4 Numerical Implementation and Results

A specific test case is chosen with $A = R = \alpha = n = 1$. Since the test case has a periodicity of 2π along the cylinder, the infinite integration in q may be replace by a finite range through the use of the method of images. Specifically,

$$\int_{-\infty}^{\infty} K(p,q)\,\mathrm{d}q = \int_{\zeta-\pi}^{\zeta+\pi} \sum_{k=-\infty}^{\infty} K(p,q+2k\pi)\,\mathrm{d}q. \quad (48)$$

Ewald summation is used to accelerate the convergence of this sum; see the Appendix.

The surface parameters p and q are divided into N and M evenly spaced intervals with spacings $h_1 = 2\pi/N$ and $h_2 = 2\pi/M$ and the integrals evaluated according to the descriptions of the previous sections, but some additional details should be mentioned. During the evaluation of the integrals (19), the range in ρ can lead to points outside the ranges $0 < p < 2\pi$ and $0 < q < 2\pi$. Values of quantities at these points can be obtained by periodic extensions of their values inside the periodic box. On the other hand, it is more convenient to perform the integrations in p, q of the second integral in (21) centered on (η,ζ). Provided $r_2 < \pi$, only the term $k = 0$ may be affected by $T(\rho)$. This observation has impact on the Ewald summation as presented in the Appendix.

The maximum absolute error on the surface in the numerical calculation of the velocity (14) is shown in Fig. 2 for various choices of the grid spacings and the choice of $K = M$ for the number of intervals in θ. The evidence is strong that ln(error) is decreasing linearly in M when large enough, and hence the method is

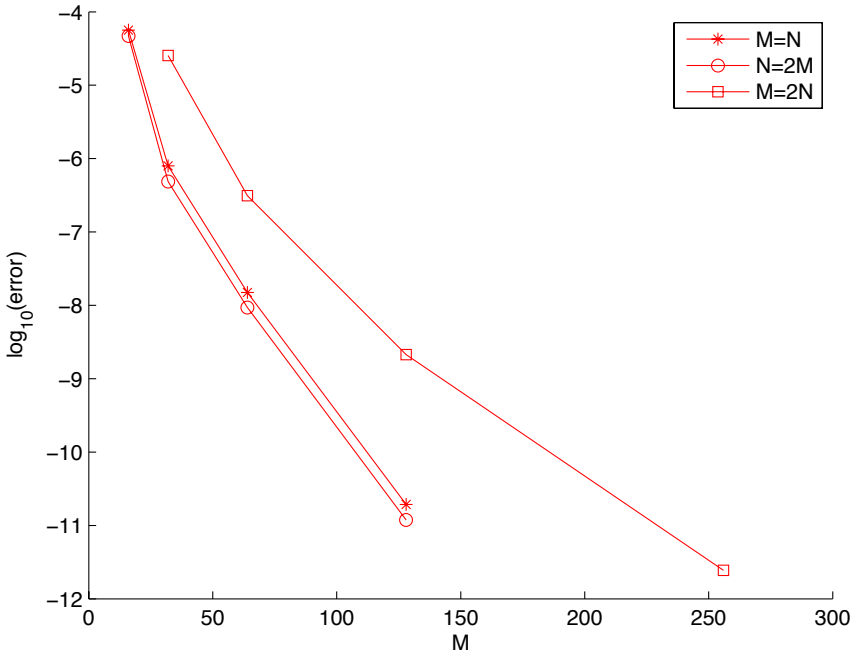

Figure 2: Maximum absolute error for different grid sizes

exponentially accurate. The case $M = 2N$ has slightly worse errors and is due to the lower number of points in the azimuthal angle p. Keeping the spacing comparable in size seems to provide the best results. Also the spacing in θ must decrease as the same rate as h_1 and h_2 in order to see spectral accuracy.

The exponential rate of convergence does not depend on the range in the transition function as demonstrated in Fig. 3. The results from the selection of ranges suggest that its width $r_2 - r_1$ is the most important factor. More experimentation would be helpful in further clarifying the choice of the transition function and its influence on the errors, but the indications are that he results do not depend sensitively on the choice of r_1 and r_2.

5 Conclusion

Converting the surface integration into polar coordinates allows a spectrally accurate calculation of the surface integral typically found in applications of boundary integral methods for free surface flow. The approach does require interpolation but

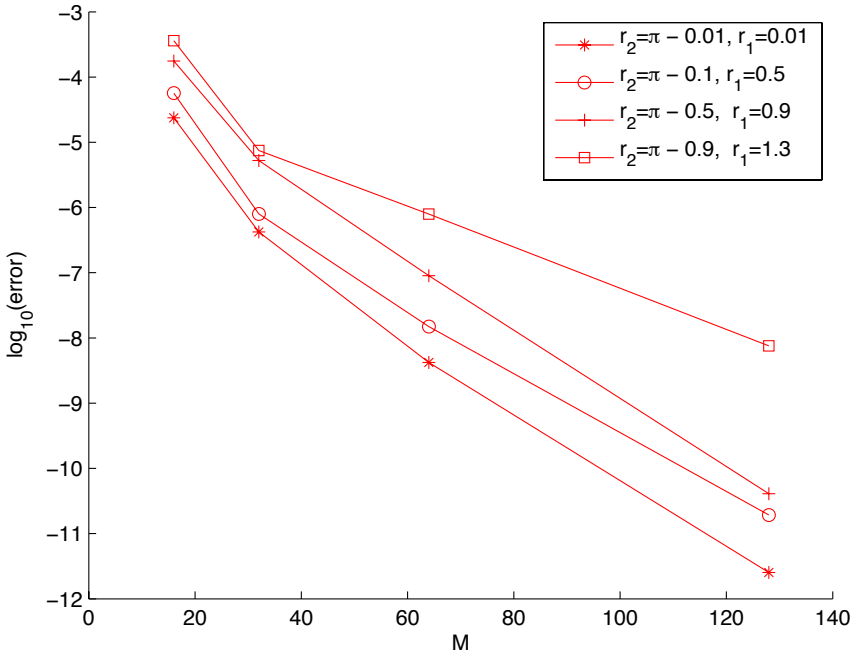

Figure 3: Maximum absolute error for different transition zones.

by performing the integration first in the radial coordinate it is possible to restrict all interpolations to locations on grid lines, thus limiting the costs. Employment of a transition function also reduces the amount of interpolation to a disk around the point of singularity in the integrand.

6 Appendix

Ewald summation helps reduce the cost of evaluation of the sums that result from the method of images. Specifically, the required sum is

$$G^{\pi} = -\sum_{m=-\infty}^{\infty} \frac{1}{4\pi r_m} \tag{49}$$

where

$$r_m^2 = R^2 + (z - 2m\pi)^2, \quad R^2 = x^2 + y^2.$$

For $R/(2\sqrt{\pi} < 1$, the Poisson summation formula produces

$$G^{\pi} = -\frac{\gamma+2\ln(\sqrt{\pi})}{8\pi^2} - \sum_{m=-\infty}^{\infty} \frac{1}{4\pi r_m} \operatorname{erfc}\Big(\frac{r_m}{2\sqrt{\pi}}\Big) - \frac{1}{4\pi^2} \sum_{m=1}^{\infty} E_1(m^2)\cos(mz) - \frac{1}{8\pi^2} \sum_{n=1}^{\infty} \frac{(-1)^n}{n!} \Big(\frac{R}{2\sqrt{\pi}}\Big)^{2n} \sum_{m=0}^{\infty} \varepsilon_m E_{n+1}(m^2)\cos(mz) \quad (50)$$

where γ is Euler's constant, $\varepsilon_0 = 1$, $\varepsilon_m = 2$ for $m \geq 1$ and

$$E_n(x) = \int_1^{\infty} t^{-n} \mathrm{e}^{-xt}\, \mathrm{d}t$$

is the exponential integral. The exponential function decreases exponentially as $x \to \infty$ and the sums in (50) converge quickly.

For $R/(2\sqrt{\pi} > 1$, the eigenfunction expansion for G^{π} can be used;

$$G^{\pi} = \frac{1}{4\pi^2} \ln\Big(\frac{R}{2\pi}\Big) - \frac{1}{2\pi^2} \sum_{m=1}^{\infty} K_0(mR)\cos(mz) \quad (51)$$

where $K_0(x)$ is the modified Bessel function which decays exponentially as $x \to \infty$. Because of the presence of $T(\rho)$ in the second integral of (21) and the range of integration in q, the required sum for the integrals in (48) can be evaluated by using

$$-\sum_{m=-\infty}^{\infty} \frac{1-T(\rho)}{4\pi r_m} = -\frac{1-T(\rho)}{4\pi r_0} + G^{\pi} + \frac{1}{4\pi r_0} \quad (52)$$

Acknowledgement: The research was supported by NSF (grant OCE-0620885).

References

Beale J.T. (2001): A convergent boundary integral method for three-dimensional water waves, *Math. Comput.*, 70, p. 977.

Baker G.R. (2010): *Boundary Element Methods in Engineering and Sciences*, Chapter 8, Imperial College Pres.

Saffman P.G. (1992): *Vortex Dynamics*, Cambridge University Press.

Baker G.R. (1982): D.I. Meiron and S.A. Orszag, Generalized vortex methods for free-surface flow problems, *J. Fluid Mech.*, 123, pp. 477–501.

Baker G. R., Meiron D. I., Orszag S. A. (1984): Boundary integral methods for axi-symmetric and three-dimensional Rayleigh-Taylor instability problems, *Physica* 12D.

Baker G.R., Beale J.T. (2004): Vortex blob methods applied to interfacial motion, *J. Comput. Phys.*, 196, 2004, pp. 233–258.

Baker G.R., Zhang H. (2010): Blob regularization of boundary integral integrals, in Advances in Boundary Element Techniques XI, Berlin, Germany.

Bruno O., Kunyansky L. (2001): A fast, high-order algorithm for the solution of surface scattering problems: basic implementation, tests, and applications, *J. Comput. Physics*, 169, p. 80.